Available online at www.sciencedirect.com
SCIENCE DIRECT
International Journal of Heat and Fluid Flow 27 (2006) 707–720
International Journal of HEAT AND FLUID FLOW
www.elsevier.com/locate/ijhff

Computational analysis of locally forced flow over a wall-mounted hump at high-*Re* number

S. Šarić [a], S. Jakirlić [a,*], A. Djugum [b], C. Tropea [a]

[a] *Chair of Fluid Mechanics and Aerodynamics, Darmstadt University of Technology, Petersenstrasse 30, Fachbereich 16, D-64287 Darmstadt, Germany*
[b] *Department of Mechanical Engineering, University of Sarajevo, Omladinsko Šetalište 9, 71000 Sarajevo, Bosnia and Herzegovina*

Available online 23 March 2006

Abstract

An incompressible, high-Reynolds number flow (slightly less then 1 Mio. per chord) over a smoothly contoured, asymmetric, wall-mounted hump was computationally studied using the LES (large eddy simulation) and DES (detached eddy simulation) methods. In addition, several second-moment and eddy-viscosity closures within the RANS (Reynolds-averaged Navier–Stokes) framework were tested. The focus of the investigation was on the effects of local perturbation of the hump boundary layer introduced by spatially uniform (in the spanwise direction) steady suction and oscillatory suction/blowing through a narrow opening (1.7 mm) situated at the hump crest immediately upstream of the natural separation point. Reference experiments have shown that both flow control mechanisms cause a shortening of the recirculation bubble relative to the baseline configuration with no flow control. All statistical turbulence models used in the RANS framework resulted in a substantially larger recirculation zone independent of the modelling level, being a consequence of a too low turbulence level in the separated shear layer. Accordingly, the effect of the steady suction, namely the reduction of the reattachment length, was underpredicted. The LES method, despite a relatively coarse mesh (with a total of 4 Mio. cells) for such a high-Reynolds number, wall-bounded flow, was capable of capturing important effects of the flow control qualitatively and quantitatively. DES failed to do so in the suction case, despite good results in the baseline and oscillatory blowing/suction cases, indicating that a shallow separation from curved surfaces poses a challenge to this hybrid RANS/LES strategy. A sensitivity study of the RANS/LES interface position within the DES approach shows that a RANS region chosen too thin (with the interface situated at the very beginning of the logarithmic layer) can lead to a strong reduction of the turbulent viscosity causing a low turbulence level within the shear layer region aligned with the recirculation zone, which in turn leads to a larger separation bubble.

Keywords: Flow separation control; Oscillatory blowing/suction; LES; DES

1. Introduction

One of the most important tasks in the fluid mechanics research, in general, is to control turbulent flow evolution with respect to overall drag reduction. Flow separation, often being consequence of an adverse pressure gradient, is certainly one of the main flow phenomena contributing to increased pressure losses. Therefore, separation delay or recirculation zone shortening is of great interest in a number of industrial branches, e.g. turbomachinery, car, aircraft aerodynamics, etc. Although passive flow control devices like airfoil vortex generators have been proven to be quite effective in delaying flow separation, under some flow conditions they may cause undesired effects, e.g. drag increase in the absence of the flow separation. On the other hand, recent experimental studies have demonstrated that active flow control has a potential to enable significant advances in many engineering applications. There are different methods of turbulent flow control; the most common are steady flow suction and periodic flow

* Corresponding author. Tel.: +49 6151 16 3554; fax: +49 6151 16 4754.
E-mail address: s.jakirlic@sla.tu-darmstadt.de (S. Jakirlić).

0142-727X/$ - see front matter © 2006 Elsevier Inc. All rights reserved.
doi:10.1016/j.ijheatfluidflow.2006.02.015

perturbation at the natural separation point. Whereas steady momentum injection (blowing) is not widely used mainly due to its inefficiency, numerous experimental studies of unsteady flow control show that periodic excitation, i.e. an alternating zero-net-mass flux blowing/suction, can be more efficient than steady blowing and at least as effective as steady suction. As examples, the following experimental investigations are noted: flows with a fixed separation point – flow over a backward-facing step (Chun and Sung, 1996; Jin et al., 2001; Yoshioka et al., 2001) – and separation from smooth surfaces – flow past an airfoil and over a hump (Seifert and Pack, 1999, 2002). The obvious advantage of periodic forcing is lower energy consumption in comparison to the other two methods. Oscillatory perturbation, if introduced into a separating turbulent boundary layer, is expected to increase the turbulence level in the shear layer; a higher level of the shear stress implies a higher momentum transport across the shear layer and consequently separation delay and shortening of the recirculation bubble. However, the underlying flow physics and different mechanisms responsible for an efficient flow control are not fully understood. The aforementioned flow configurations have recently attracted attention of the CFD community. The periodically perturbed backward-facing step flow (Yoshioka et al.) served as a test case at the 9th ERCOFTAC workshop on refined turbulence modelling (Jakirlić et al., 2002) and was recently computationally investigated by Šarić et al. (2005) and Dejoan et al. (2005). The turbulent flow over a wall-mounted hump (Fig. 1, simulating the upper surface of a Glauert–Goldschmied type airfoil at zero angle of attack) at a high-Reynolds number of $Re_c = 9.36 \times 10^5$ (based on the free-stream velocity $U_\infty = 34.6$ m/s and the chord length $c = 0.42$ m) situated in a plane channel (height $0.909c$) was experimentally re-examined at the NASA Langley Research Center (Greenblatt et al., 2004, 2005) for the purpose of the CFDVAL workshop on computational methods and turbulence models validation (Gatski and Rumsey, 2004). The same test case was studied at the 11th ERCOFTAC workshop on refined turbulence modelling (Johansson and Davidson, 2005). Hereby, three flow configurations were investigated: steady flow with no control (baseline) and two cases with flow control accomplished by steady suction through a thin slot ($0.004c$ wide) situated at approximately 65% of the chord length, immediately upstream of the natural separation point, as well as by an alternating suction/blowing (zero net-mass-flow rate) of a jet into the boundary layer. The oncoming flow is characterized by a zero-pressure-gradient turbulent boundary layer, whose thickness δ is approximately 57% of the maximum hump height ($h_{\max} = 53.74$ mm) measured at the location about two chord lengths upstream of the hump leading edge (coinciding with the origin of the coordinate system, Fig. 1), corresponding to the momentum-thickness-based Reynolds number $Re_\theta \approx 7500$. The latter result was obtained by applying a near-wall, second-moment closure model, Fig. 2.

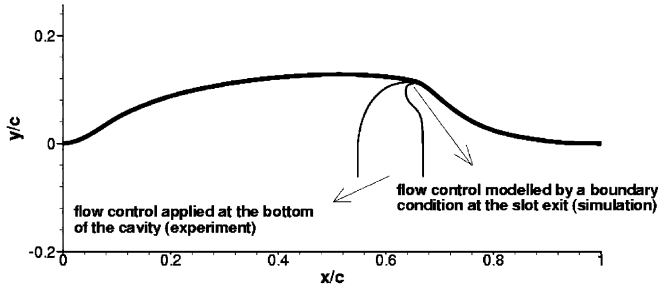

Fig. 1. Schematic of the hump geometry.

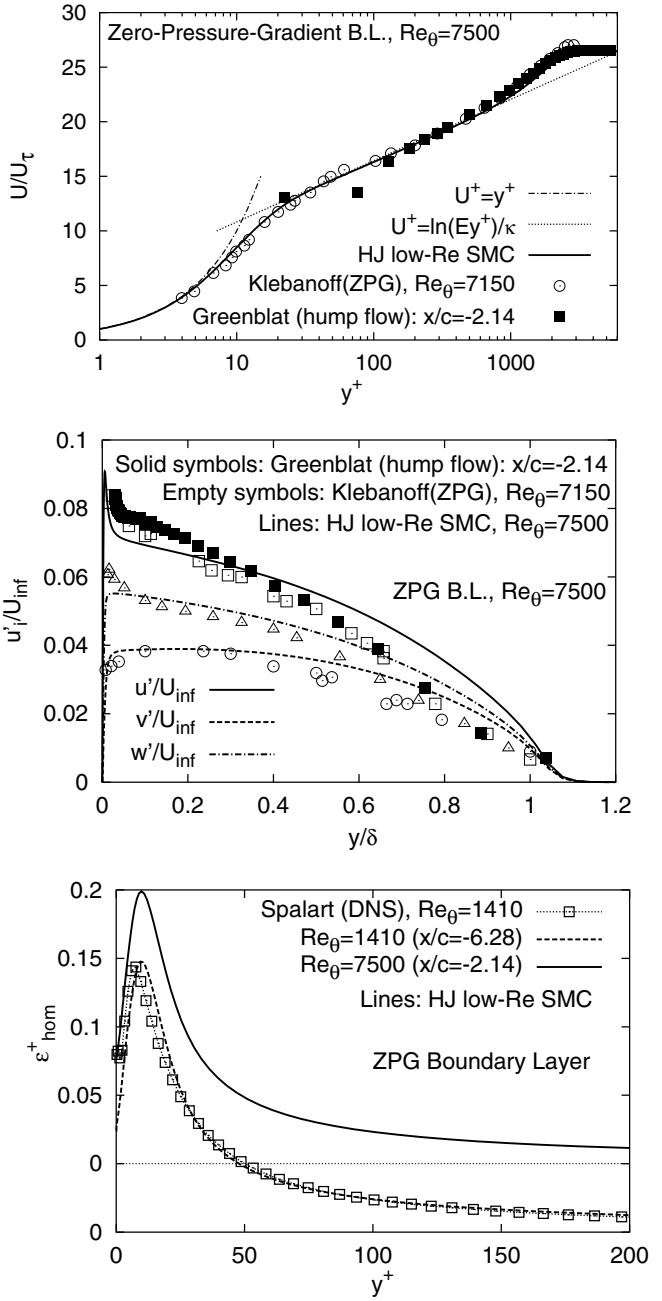

Fig. 2. Mean velocity, Reynolds stresses and dissipation rate at location $x/c = -2.14$ corresponding to the zero-pressure gradient boundary layer at $Re_\theta = 7500$. $\varepsilon_{\text{hom}} = \varepsilon - 0.5\mathscr{D}_k^v$.

Though demonstrated experimentally, unsteady flow separation, featured by the organized, large-scale coherent structures (characterized by both repeatable, but also non-regular unsteadiness of the oscillatory separated regions), remains a challenge for numerical simulation strategies. All three hump flow configurations including both separation control modes, i.e. steady suction and oscillatory blowing/suction, were considered in the present work.

The major issue of the present paper was a computational study of the effects of the boundary layer forcing on the mean flow and turbulence providing a comparative analysis of various methods for unsteady flow computations: large eddy simulation (LES), detached eddy simulation (DES), and Reynolds-averaged Navier–Stokes method (RANS; both major model groups, eddy-viscosity models – EVM and differential second-moment closure models – SMC, were applied employing both approaches for near-wall treatment: standard wall functions and integration of the governing equations through the viscous sublayer and buffer layer) in such a complex flow situation.

2. Computational method

All computations were performed with an in-house computer code FASTEST 3D (flow analysis by solving transport equations simulating turbulence) based on a finite volume numerical method for solving both three-dimensional filtered and Reynolds-averaged Navier–Stokes equations on block-structured, body-fitted, non-orthogonal meshes. Block interfaces are treated in a conservative manner, consistent with the treatment of inner cell-faces. A cell centered (collocated) variable arrangement and cartesian vector and tensor components are used. The well-known SIMPLE algorithm was applied for coupling the velocity and pressure fields. The computer code is parallelized applying the message passing interface (MPI) technique for communication between the processors. The sub-grid scales in the LES were modelled by the most widely used model formulation proposed by Smagorinsky (1963) with $C_s = 0.1$. A one-equation turbulence model by Spalart and Allmaras (S-A, 1994), based on the transport equation for turbulent viscosity, was employed to model the influence of the smallest, unresolved scales on the resolved ones within the DES computational scheme (e.g. Travin et al., 2002). The DES represents the most prominent, continuous hybrid RANS/LES method, with no necessity for explicit treatment/specification of the flow variables in the region of interface. The above-mentioned S-A turbulence model was also applied in the RANS mode. It was interesting to see how the same model performed in two different computational frameworks: RANS and DES. Various statistical turbulence models were examined by computing the baseline and steady-suction cases. They include the standard high-Reynolds number k–ε model and its near-wall adaptation due to Launder and Sharma (LS k–ε; 1974) as well as the low-Reynolds number Reynolds-stress model developed by Hanjalić and Jakirlić (HJ RSM; 1998) employing the homogeneous part of the total viscous dissipation rate as a scale-supplying variable (Jakirlić and Hanjalić, 2002) and its high-Reynolds number asymptote due to Gibson and Launder (GL RSM; 1978). The length scale correction proposed by Hanjalić and Jakirlić (1998) was introduced in the latter models to prevent the back-bending of the mean dividing streamline at the reattachment. For the sake of brevity no model specification will be given here. Potential readers should consult the original references for more details.

The convective transport of all variables was discretized by a second-order, central differencing scheme (CDS) when performing LES, DES and RANS-EVM calculations. In the case of the Reynolds-stress model computations a blended first-order-upwind/second-order-central differencing scheme, implemented in a deffered-correction manner, was applied with the value of blending factor 0.7 corresponding to the CDS scheme. Time discretization was accomplished by applying the (implicit) Crank–Nicolson scheme.

2.1. Solution domain and computational grid

The solution domain (dimensions: $L_x \times L_y \times L_z = 6.14c \times 0.909c \times 0.152c$) was meshed with almost 4 Mio. ($426 \times 145 \times 64$) grid cells when applying LES. A grid used in the 2D RANS calculations (426×145) was extruded in the spanwise direction to create 3D grid configurations used for LES and DES. The solution domain employed for DES with a somewhat larger spanwise dimension ($L_z = 0.2c$) was meshed by approximately 1.7 Mio. ($426 \times 145 \times 28$) grid cells. The RANS computations (not presented here) have not shown significant difference in the solutions obtained if the computation domain was extended further upstream ($6.39c$) as in the experiment.

2.2. Inflow conditions

It has been demonstrated experimentally that the flow is insensitive to the upstream boundary conditions. Therefore, in all LES and DES computations available steady profiles (the mean experimental velocity profiles) were imposed at the inlet plane placed at $2.14c$ upstream of the hump leading edge, Fig. 2. This is in accordance with the results of the CFDVAL workshop on computational methods and turbulence model validation (Gatski and Rumsey, 2004). The Reynolds-stress model computations require more elaborated profiles of all turbulence quantities including the dissipation rate of the turbulent kinetic energy at the inlet cross-section (note that only the profiles of the mean velocity and streamwise stress component were available from the reference experiment). For this purpose, the inflow data were generated by doing a separate computation of the zero-pressure gradient (ZPG) boundary layer with the same free-stream velocity $U_\infty = 34.6$ m/s, using the same near-wall second-moment closure model (denoted by HJ low-Re SMC). The profiles obtained at the

streamwise location corresponding to the boundary layer thickness $\delta = 30.5$ mm ($Re_\theta \approx 7500$, Fig. 2), being in accordance with the experimental results at $x/c = -2.14$, were taken finally at the inlet plane of the solution domain for the hump flow computations. The obtained results show good agreement with the available experimental data of Greenblat et al. In addition, the results of the boundary-layer measurements performed by Klebanoff (1954) at the location corresponding to $Re_\theta = 7150$ are also displayed, confirming the ZPG boundary-layer structure of the flow at this location. Fig. 2 (lower) shows the profile of the homogeneous dissipation rate which differs from the total viscous dissipation rate only in the immediate wall vicinity (up to $y^+ \approx 20$) by one half of the molecular diffusion of the kinetic energy of turbulence: $\varepsilon_{\text{hom}} = \varepsilon - 0.5\mathscr{D}_k^v$. In order to quantify this computational result at such a high Reynolds number $Re_\theta \approx 7500$ (solid line in Fig. 2), for which no reference data (neither experimental nor from a DNS) exist, the profile obtained at an upstream location $x/c = -6.28$ corresponding to $Re_\theta = 1410$ was compared with the direct numerical simulation (DNS) of Spalart (1988), exhibiting very good agreement. The latter comparison is important with respect to the credibility of the dissipation rate prediction. It should be noted that the energy dissipation rate obtained by this near-wall SMC model was also used for the resolution assessment (see Fig. 3).

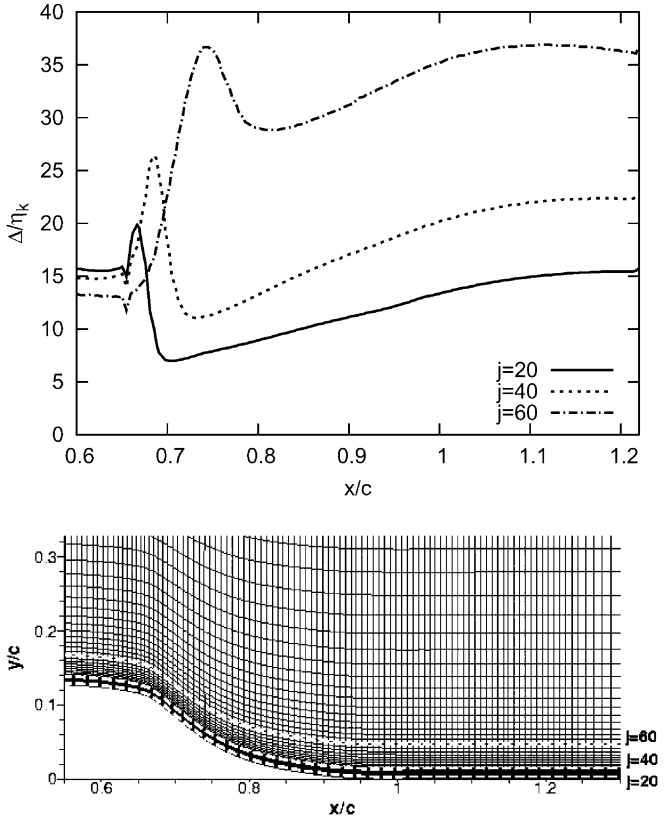

Fig. 3. Ratio of the grid scale to the Kolmogorov length scale and locations of the grid resolution assessment.

2.3. Boundary conditions and time step

A further important outcome of the CFDVAL workshop was that the modelling of the flow within the cavity/nozzle (Fig. 1) was not found to be critical for the flow predictions, as far as the baseline and steady suction flow control cases are concerned. Although there is no forced flow within/through the cavity in the baseline case, the experiment was performed using the opened slot. Accordingly, a low-speed flow through the cavity opening could be generated due to the pressure difference. However, the S-A RANS computation of the baseline case, though not shown here, has shown that modelling of the cavity opening did not result in noticeable differences compared to the results presented here. Consequently, different flow configurations have been computed by imposing the appropriate boundary conditions directly at the control slot. Steady suction was achieved by adopting the spatially uniform suction velocity at the slot corresponding to the mass flow rate of 0.01518 kg/s. Oscillatory suction/blowing was simulated by imposing a sinusoidal zero net-mass-flow jet at the slot with the frequency of 138.5 Hz. Different velocity amplitudes were examined. If the measured peak slot velocity of 26.6 m/s was taken, the resulting mass flow rate was twice as high as the experimental value. Hence, a more realistic boundary condition was to impose the slot velocity corresponding to the experimental mass flow rate. Interestingly, boundary conditions in the oscillatory case were not influential as far as the gross flow characteristics like locations of flow separation and reattachment are concerned. However, the latter boundary condition turned out to be more adequate, yielding superior predictions of the flow velocity and turbulence field.

No-slip boundary conditions were applied at both walls resolving the wall boundary layer when performing LES and DES. The dimensionless wall distance y^+ of the wall-closest computational nodes were $y^+ < 1$ for the lower wall and $y^+ = 1.0$–1.75 for the upper wall. The values of y^+ of the wall-nearest grid point were between 0.5 for the low-Re number, RANS calculations and $\geqslant 15$ for the high-Re number, RANS calculations. In the case of the high-Re number, RANS computations the standard wall functions have been applied. In the case of LES and DES, the convective outflow conditions were applied at the outlet and periodic boundary conditions along the spanwise direction.

The dimensionless time steps of 0.005 and 0.003 (based on the hump chord length and free stream velocity) were used in the DES and LES, respectively, providing a CFL number less than unity throughout the largest portion of the solution domain. The only exception was the narrow region around the thin slot at the hump (1.7 mm wide) in the oscillatory blowing/suction case, where a high velocity jet was introduced into the separated shear layer. The CFL number reaches its maximum value being around 15 in a very few cells in this region which is characterized by a strongly refined grid. Additionally, some preliminary simulations of the oscillatory blowing/suction case employing

finer time steps (0.0016 and 0.003) revealed that the results were not significantly affected by the time step refinement.

2.4. Grid density study

The flow region of interest just downstream of the slot including the region around the reattachment was meshed to provide $\Delta x^+ = 80$, $\Delta y^+ = 1 - 80$, $\Delta z^+ = 150$. The latter value applies to the DES grid. Compared to DES, the LES resolution was significantly finer with $\Delta z^+ = 50$ because of the finer grid ($N_{z,\mathrm{LES}} = 64$ vs. $N_{z,\mathrm{DES}} = 32$) and a somewhat smaller spanwise domain size ($L_{z,\mathrm{LES}} = 0.152c$ vs. $L_{z,\mathrm{DES}} = 0.2c$). Admittedly, the grid resolution adopted is coarser than it would be required for resolving the near-wall streaky structures, which demands a spacing of order $\Delta y^+ = \mathrm{O}(1)$, $\Delta x^+ = \mathrm{O}(50)$ and $\Delta z^+ = \mathrm{O}(20)$, e.g. Hanjalić (2005). The reason for the slightly extended spanwise dimension $L_{z,\mathrm{DES}} = 0.2c$ was to shift the RANS/LES interface away from the wall in order to provide its optimal position for the given grid size, i.e. to avoid that the interface penetrates too deeply into the boundary layer. If the LES region would reside too close to the wall due to insufficient resolution (one would have actually a resolution typical for RANS in the LES region), lower viscosity and turbulence levels could be obtained, possibly causing a premature separation and poorer flow predictions. It should be recalled here, that the interface position d corresponds to the DES-filter ($C_{\mathrm{DES}}\max(\Delta x, \Delta y, \Delta z)$); $C_{\mathrm{DES}} = 0.65$, Travin et al. (2002).

The ratio of the grid length scale to the Kolmogorov length scale (Δ/η_k; $\eta_k = (\nu^3/\varepsilon)^{1/4}$), representing to a certain extent the position of the cut-off in the frequency spectra, is displayed in Fig. 3. Three positions along the gridlines in the streamwise direction are considered, two of which reside in the near-wall region ($j = 20, 40$), whereas location $j = 60$ corresponds to the separated shear layer (Fig. 3). The Kolmogorov length scale was estimated from the dissipation rate obtained from the RANS computation of the baseline case employing the Reynolds stress model formulation of Hanjalić and Jakirlić (1998). In absence of the turbulence-energy budget, the dissipation rate obtained from the second-moment closure can provide insight into the grid resolution (see Fig. 2 (lower) to check the capability of the HJ RSM model to capture dissipation profile correctly). Based on this assessment it appears that the near-wall region has a sufficient resolution for LES (ideally, the value $\leqslant$10–12 would provide the spectral cut-off being fairly close to the high-frequency wave-number range, corresponding to the dissipative part of the spectra, Fröhlich et al., 2005; Dejoan et al., 2005), while the grid resolution in regions away from the walls, including the separated shear layer, seems to be coarser. However, the employed resolution still provides modelled turbulent kinetic energy (estimated as $k_{\mathrm{sgs}} = \Delta^2|S|^2/0.3$, according to Mason and Callen, 1986) which does not exceed 5–9% of the resolved one and the ratio of the instantaneous SGS viscosity to the molecular one remains typically between 5 and 13 (maximum values apply within the region around the hump).

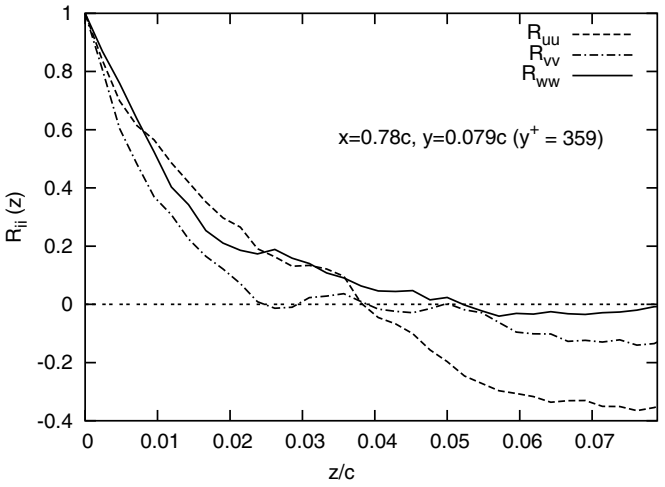

Fig. 4. Spanwise autocorrelation functions R_{uu}, R_{vv} and R_{ww} obtained by LES (baseline case) along a spanwise line within the separated shear layer at $y/c = 0.079$ ($y^+ = 359$) at the streamwise location $x/c = 0.78$ corresponding to the middle of the separation bubble.

The spanwise autocorrelation functions R_{uu}, R_{vv} and R_{ww} obtained by LES along a spanwise line within the separated shear layer at $y/c = 0.079$, i.e. $y^+ = 359$, at the streamwise location $x/c = 0.78$ (corresponding to the middle of the separation bubble) are plotted in Fig. 4 in order to check the adequacy of the spanwise size of the solution domain. The spanwise extent of the vortical structures corresponds approximately to double the value of the correlation length representing the distance between the origin and the separation where the correlations drop off to zero. Apart from the correlation of the w fluctuations, the correlations remain at 15–35% at the largest separation ($z/c = 0.075$). Such an increased correlation length is typically a consequence of the spanwise rollers in the shear layer. This analysis provides a clear indication that the correlations do not vanish within the half of domain size in the spanwise direction. Therefore, the adopted spanwise dimension is not entirely sufficient to ensure spanwise decorrelation. The spanwise extent adopted in the detached-eddy simulation is somewhat larger ($L_{z,\mathrm{DES}} = 0.2c$). Looking at the plots representing iso-surfaces of the streamwise and spanwise vorticity in Section 3.3 it could be regarded as sufficient. It should be furthermore noted that the main objective of the work was comparative analysis of the most widely used method for unsteady flow calculations, such as LES and DES, and they both were performed under comparable conditions. Let us just note, that some other authors (see e.g., Krishnan et al., 2004) have used a substantially smaller spanwise dimension ($L_z = 0.121c$) to perform DES of the hump baseline flow.

3. Results and discussion

Flow statistics were taken over 5–7 flow-through times and the time-averaged results were extracted to provide

comparison with the available experimental data. The results displayed comprise the wall pressure distribution, time-averaged streamlines, corresponding profiles of mean velocity field and turbulence quantities at characteristic locations within the separation zone and post-reattachment region, as well as the instantaneous flow field: velocity field, pressure fluctuations, spanwise and streamwise vorticity.

The separation and reattachment locations for the computed configurations are summarized in Table 1 and Fig. 5. The effect of the flow control on the recirculation zone shortening can be clearly recognized. Both the LES and DES (apart from the steady suction case) results are in a very close agreement with the reference experiment with respect to both separation and reattachment locations. The experimental observation, that the steady suction represents the most effective flow control mode, that is the case with the minimum reattachment length, was confirmed by both computational methods. These results will be discussed in more details in the following sections. The predictions of the separated flow over a wall-mounted hump for the configurations without flow control (baseline) and steady suction flow control will be discussed first. Afterwards, some results for the case with oscillatory (sinusoidal) suction/blowing flow control will be presented as well.

3.1. Baseline configuration

Predictions of the pressure coefficient for the baseline case are shown in Fig. 6. The LES and DES results agree better with the measurements than the 2D S-A RANS ones. However, the peak suction pressure is underpredicted with all methods. This can be partially explained by possible blockage effects from the wind tunnel side walls, not accounted for in the computations. The mean streamwise velocity profiles are shown in Fig. 7. All RANS models overpredict significantly the reattachment length in spite of (partially) correct capturing of the separation location (see Table 1 for the quantitative comparison). The LES and DES results agree well with the experimental data. It is interesting to see that DES predictions are even better than the ones obtained by the conventional LES especially in the region of the velocity profile inflection, that is the region with zero value of its second derivative (see also the shear stress profiles in Fig. 8). The reason for such an outcome can be justified by a more suitable modelling of the oncoming wall boundary layer (near-wall Spalart-Allmaras model in the DES framework vs. mixing-length-hypothesis-based Smagorinsky model), the fact coming

Table 1
Separation and reattachment locations

	$(x/c)_S$	$(x/c)_R$
Baseline		
Exp.	0.673	1.110
LES	0.667	1.114
DES	0.663	1.121
S-A	0.667	1.259
Std. k–ϵ	0.672	1.125
LS k–ϵ	0.670	1.125
GL RSM	0.670	1.158
HJ RSM	0.660	1.195
Suction		
Exp.	0.686	0.940
LES	0.671	0.947
DES	0.674	1.105
S-A	0.674	1.098
Std. k–ϵ	0.684	1.005
LS k–ϵ	0.683	0.988
GL RSM	0.680	1.032
HJ RSM	0.670	1.073
Oscillatory		
Exp.	≈ 0.677	≈ 1.0
LES	0.671	1.050
DES	0.662	1.110

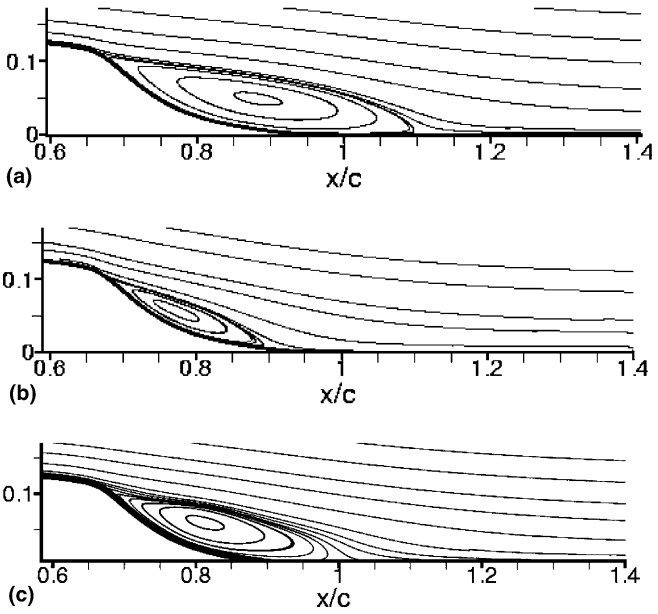

Fig. 5. Time-averaged streamlines obtained by LES method. (a) Baseline configuration, (b) steady suction configuration and (c) oscillatory suction/blowing configuration.

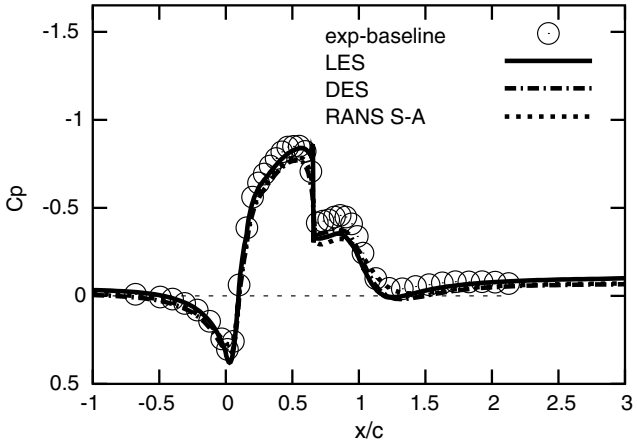

Fig. 6. Pressure coefficient for the baseline configuration.

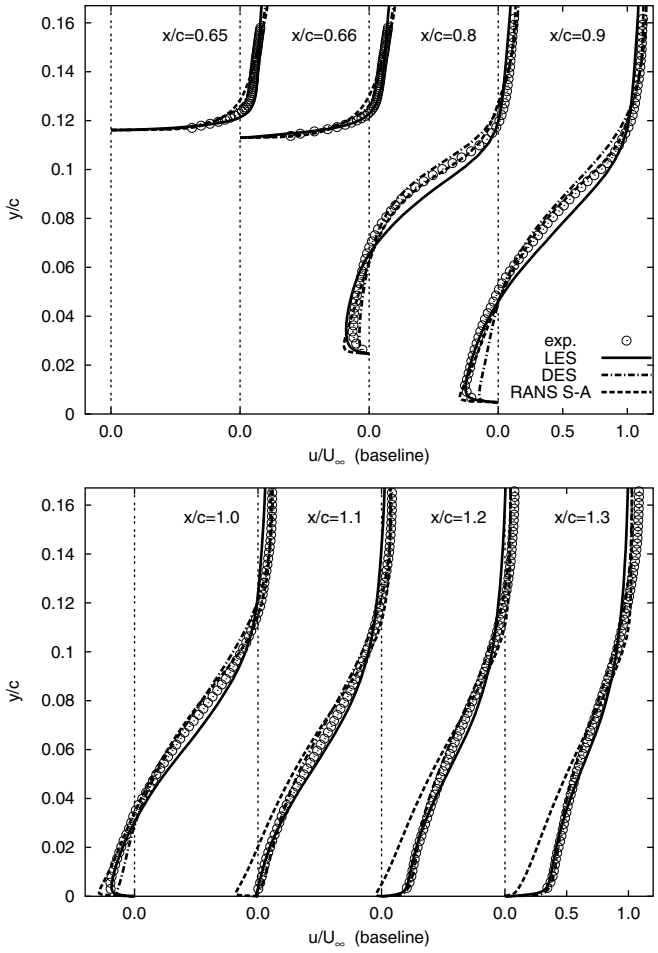

Fig. 7. Mean velocity profiles (baseline configuration).

especially into focus under conditions of a lower grid resolution. It should be noted here that the channel (height $= 0.909c \approx 381.78$ mm) constriction due to hump ($h_{\max} = 53.74$) is not too strong (only about 14%), causing the separation point as well as the separated-shear-layer structure (and consequently the size and shape of the separation zone itself) largely depend on the oncoming wall boundary layer. The feasibility of the DES as a hybrid RANS/LES approach (designed to operate as the RANS method within attached boundary layers and the LES method in detached, separated regions of the flow) is further expressed by the fact that these results were obtained using a substantially coarser grid (1.7 Mio. in total vs. 4 Mio. for LES).

The Reynolds shear stress evolution presented in Fig. 8 demonstrates how crucial it is to capture the correct level of turbulence in the separated shear layer with respect to the mean flow features downstream, especially to the reattachment location. The correct LES and DES predictions of the shear stress in the region aligned with the mean dividing streamline leads finally to the correct predictions of the reattachment length. By careful inspection of the shear stress profiles obtained by LES, one can see the influence of grid resolution in different regions of the flow. As a consequence of the under-resolved boundary layer upstream of the separation location, LES typically returns a much too high level of shear stress (locations $x/c = 0.65$ and 0.66). Likewise, due to a coarser resolution, underprediction of the shear stresses is observed downstream at $x/c > 1.0$: in the shear layer at ($x/c = 1.0$, $y/c \approx 0.08$) and in a new shear layer (where a strong interaction between the new wall boundary layer being generated in the post-reattachment region and the bulk flow occurs; cross-sections at $x/c = 1.1$, 1.2 and 1.3). The coarser grid in this region causes high dissipation and consequently lower turbulence level. Nevertheless, it is to be noted that close agreement with the measured shear stresses near the wall complies with the supposition of a sufficiently fine grid in this region. Conversely to LES, DES yields correct levels of the shear stress upstream of the separation point and consequently downstream at $x/c > 1.0$. Certain overpredictions at the locations $x/c = 0.8$ and 0.9) are likely associated with the grid resolution but one should recall that the maximum uncertainty in the measured stresses was estimated to be 20%.

Fig. 9 displays the profiles of the mean axial velocities and shear stresses, obtained by different RANS models at

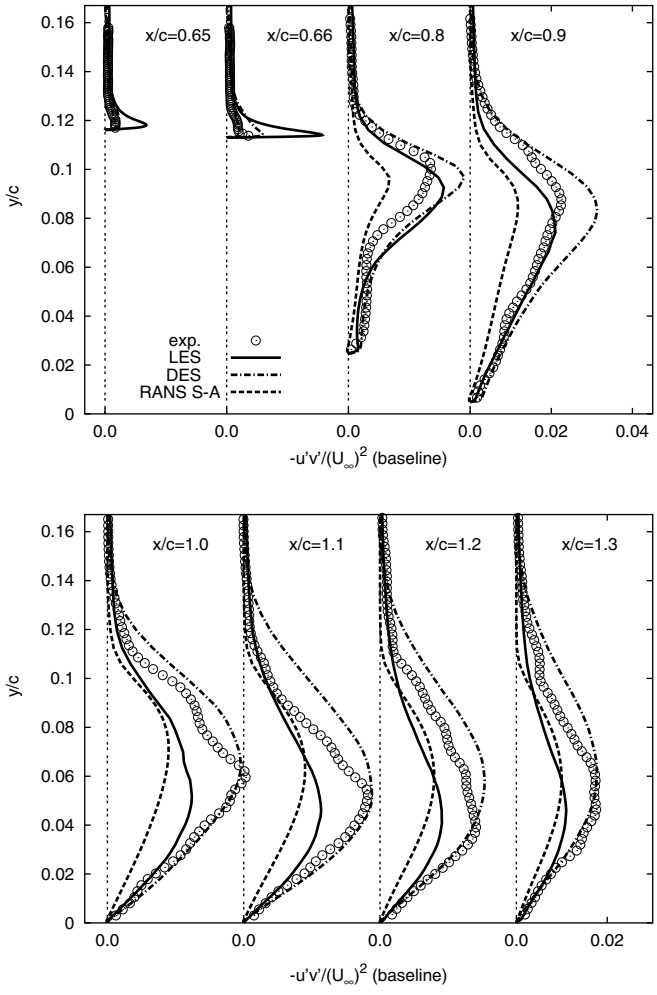

Fig. 8. Shear stress profiles (baseline configuration).

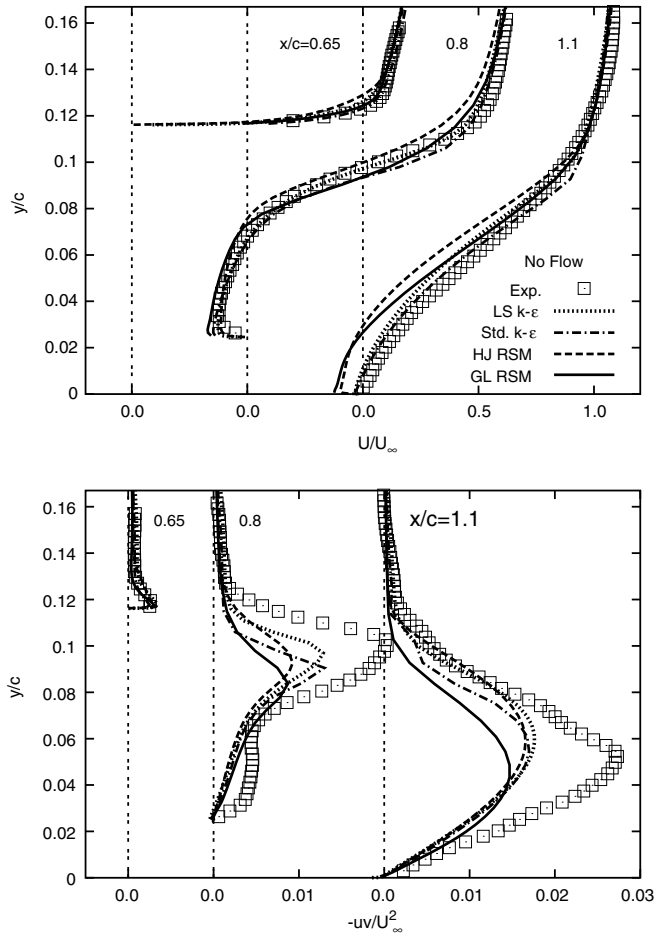

Fig. 9. Mean velocity and shear stress profiles obtained by different statistical models of turbulence (baseline configuration).

three selected streamwise locations: immediately before the separation point ($x/c = 0.65$), within the recirculation bubble ($x/c = 0.8$) and at the reattachment ($x/c = 1.1$). During the initial phase of the flow reversal up to $x/c = 0.8$ (about 90% of the entire geometry expansion occurs up to this length) a strong adverse-pressure gradient dominates the flow. This fact is responsible for the good agreement of the mean velocity profiles at $x/c = 0.8$ with respect to both the intensity of the back flow and the thickness of the separation zone, in spite of the poor prediction of the shear stresses. Further downstream at $x/c = 1.1$ the shear-stress gradient overweighs significantly the mean pressure gradient in the momentum equation. A fairly weak gradient of the shear stress components at this location, as a consequence of a generally low shear-stress level in the shear layer being aligned with the mean dividing streamline, causes a longer recirculation region. The latter is a typical outcome of the RANS method, with a fairly weak dependence on the modelling level adopted. The investigated flow configuration is characterized by unsteady separation governed by large-scale unsteadiness (highly intermittent separation and reattachment regions, highly unsteady separated shear layer), all the features being beyond the reach of the inherently steady RANS approach.

3.2. Steady suction flow control

The pressure coefficient distributions for the steady suction flow control case are presented in Fig. 10. Underpre-

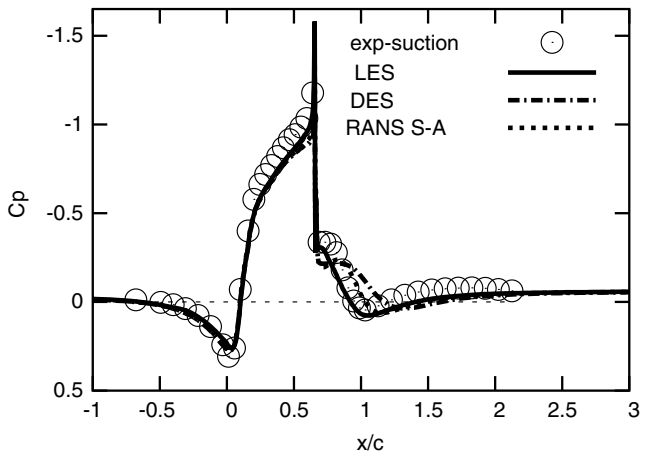

Fig. 10. Pressure coefficient for the steady suction case.

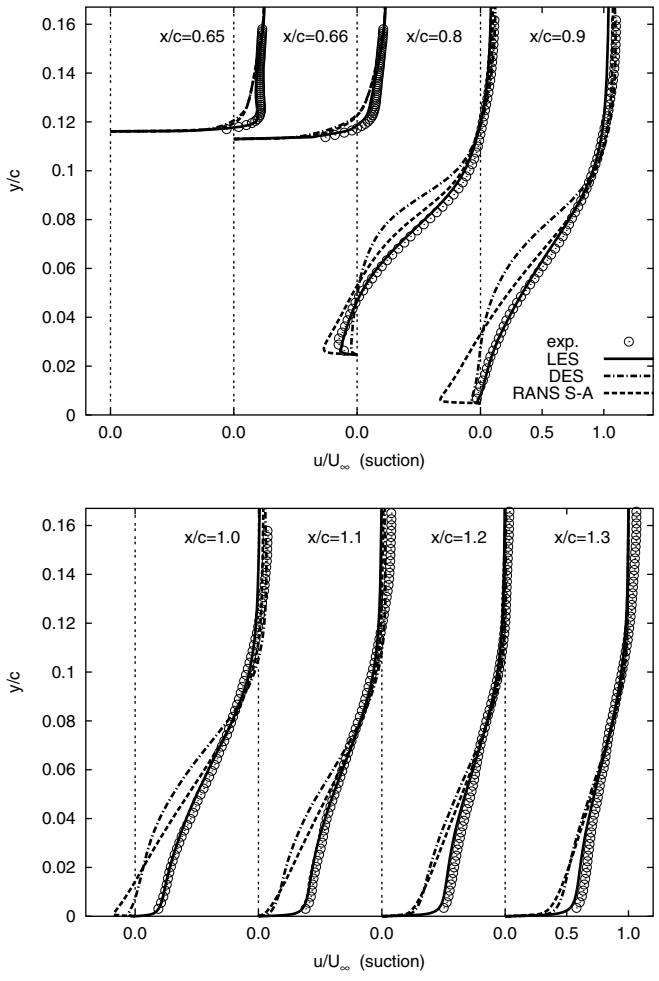

Fig. 11. Mean velocity profiles (steady suction flow control).

diction of the peak suction pressure is present in the suction case as well. Contrary to the baseline case, the advantages of the DES over the S-A RANS predictions are not observed in the pressure distributions, noting that both the RANS models and DES fail to capture the correct reattachment location, Table 1. On the other hand, LES shows in general very good agreement with the experimental data despite using the same grid as for the baseline case, which was regarded as not sufficiently fine. The reason for that can be explained by the fact, that the suction or blowing (the same is valid for the oscillatory blowing/suction case) of a high-velocity jet into the flow at a natural separation point reduces to a certain extent the necessity for a highly resolved wall boundary layer approaching the hump. For example, by activating the flow suction through a narrow opening at the hump crest, the intermittency of the separation region was damped to a large extent leading to an almost fixed separation point. The slight underprediction of the pressure coefficient along separation and recovery regions may be attributed to the aforementioned blockage effects.

Mean velocity profiles shown in Fig. 11 support the previous observation made regarding the pressure distribution. The deviations from the experimental results with respect to the back-flow intensity within the recirculation bubble are clearly visible, influencing strongly the flow around reattachment and in the recovery region downstream (it applies to S-A RANS and DES). LES predictions of the mean velocity are in very good agreement with the experiment in spite of the slightly underpredicted separation location. Reynolds shear stress profiles are presented in Fig. 12. The intensification of the mean straining due to local flow forcing in the suction case results in an enhanced turbulence level, representing the basic mechanisms behind the active flow control. Compared to S-A RANS and DES, LES captured the increased turbulence level in the separated shear layer region very well. Qualitatively different performance of the detached-eddy simulation compared to the large-eddy simulation in two different flow configurations employing the same grid (DES performs very well in the baseline case, but poorer in the suction case) indicates the importance of the grid design within the DES framework. Krishnan et al. (2004) have also reported on the poor DES predictions of the suction case compared to the baseline configuration.

The issue of the RANS/LES interface, whose position is dictated by the grid adopted (independent of the flow structure), appears to be crucial for exploiting advantages of both RANS and LES strategies in different regions of the flow. In the suction case, the position of the interface in terms of the wall units is significantly increased around the slot as shown in Fig. 13. Here, the suction control is responsible for thinning the turbulent boundary layer. It seems that the position of the RANS/LES interface needs to be shifted towards the wall to improve predictions of the flow featuring such a shallow separation. The question

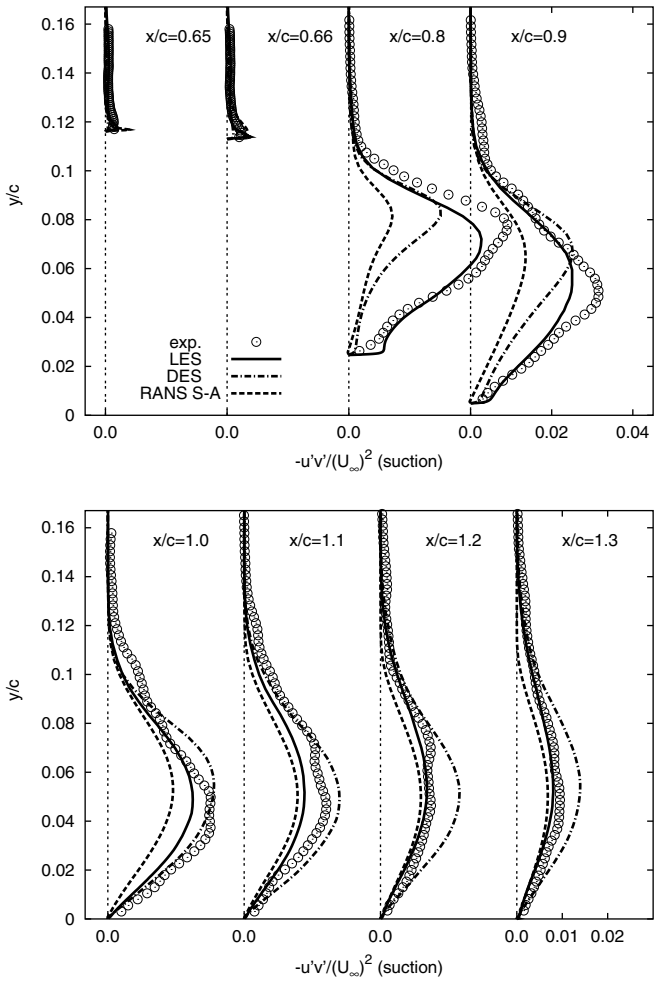

Fig. 12. Shear stress profiles (steady suction flow control).

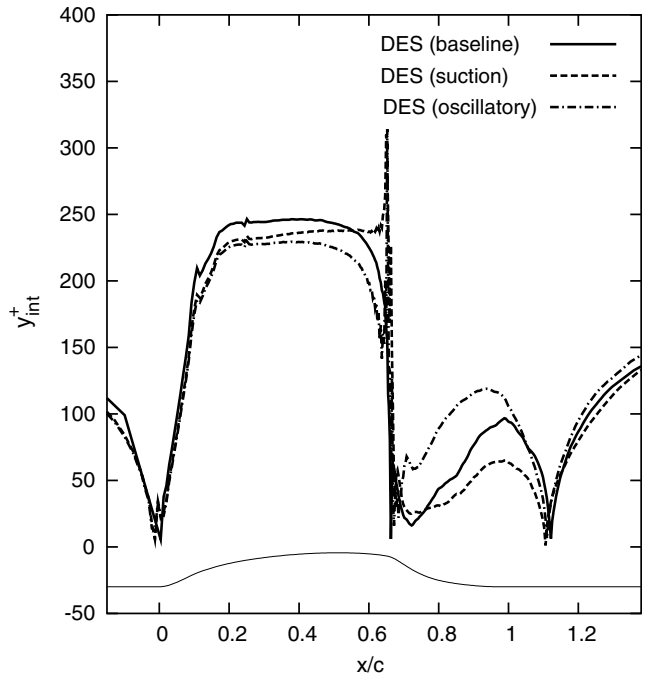

Fig. 13. RANS–LES interface in DES computations.

arising is whether the grid used for the baseline case can be used for different flow control scenarios, i.e. suction and oscillatory flow control?

3.3. Oscillatory suction/blowing flow control

In this section, some results of the oscillatory case computations will be assessed. Among the flow configurations considered, the oscillatory case appears to be the most challenging one. The control mechanism of the oscillatory case turns out to be less effective than the one of steady suction, as observed in the experiment as far as the separation delay and recirculation zone shortening are concerned (Table 1). Reattachment length reduction is reproduced by both LES and DES, but DES ovepredicts the reattachment location, similar to the suction case. Fig. 14 displays the mean axial velocity profiles at two different stations, within the recirculation region ($x/c = 0.8$) and in the recovery region ($x/c = 1.1$). The effects of the flow control on the velocity field are clearly visible. Experiments have shown that shortening of the recirculation bubble by 42% and 26%, compared to the baseline case, is achieved by applying steady suction and oscillatory flow control respectively. LES predictions are in close agreement; the same tendency of the mean velocity field is achieved (Fig. 14), while shortening of the recirculation bubble is slightly underpredicted: 38% and 25% for the two control mechanisms. LES and DES of the oscillatory case demonstrate generally good predictions of the recirculation bubble and mean flow characteristics (Figs. 15–17). It is remarkable that comparison of the mean velocity profiles at the selected stations presented in Fig. 15 reveals more accurate DES predictions compared to the suction control case.

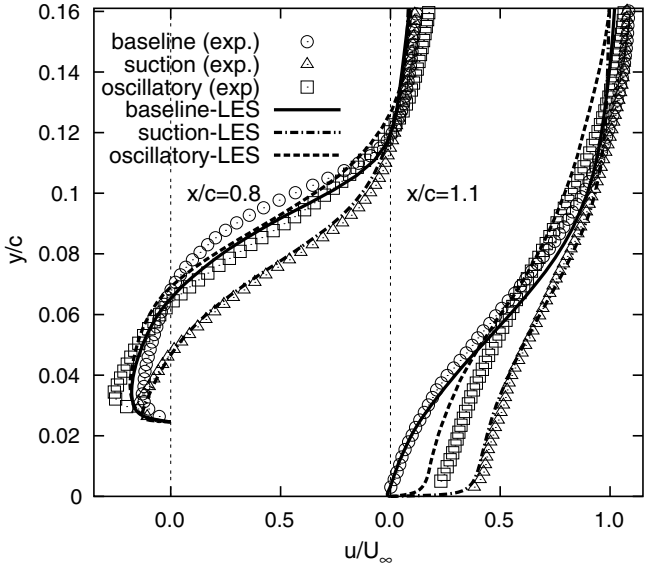

Fig. 14. Effect of the flow control on the mean velocity profiles at $x/c = 0.8$ and $x/c = 1.1$ (LES vs. experiment).

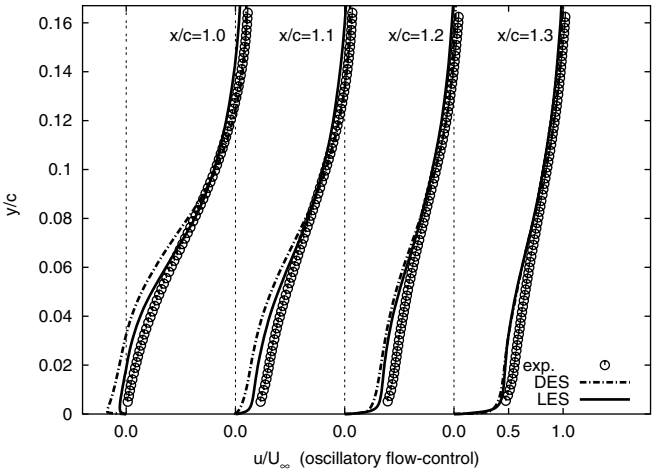

Fig. 15. Mean velocity profiles (oscillatory suction/blowing flow control).

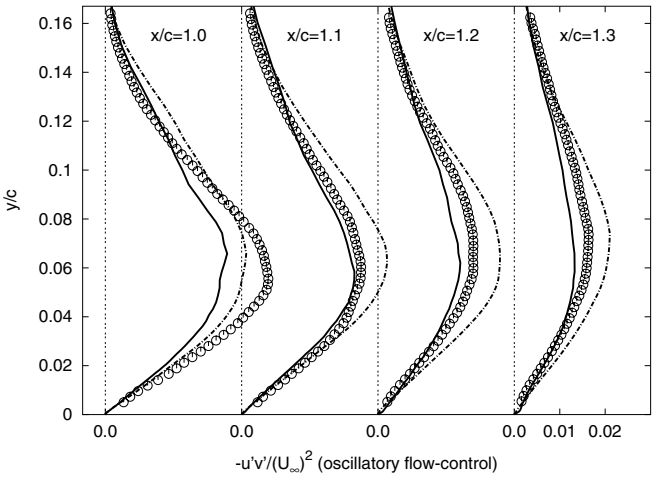

Fig. 16. Shear stress profiles (oscillatory suction/blowing flow control).

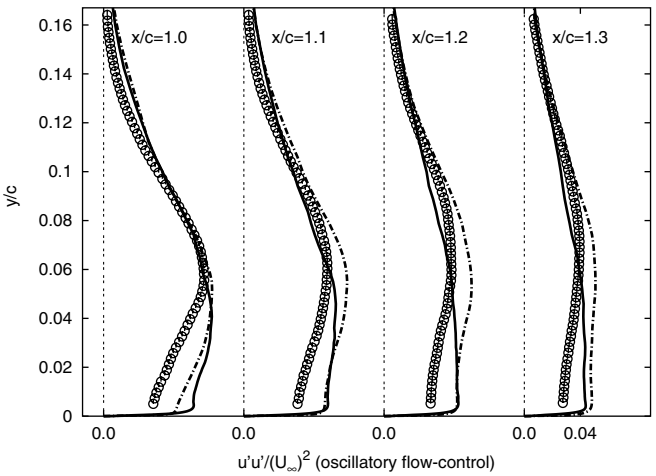

Fig. 17. Streamwise stress profiles (oscillatory suction/blowing flow control).

One of the experimentally observed features of the oscillatory case was that typically two to three vortices were present in the PIV-measurements region covering the entire separation bubble and the reattachment region up to $x/c = 1.3$ at any instant (Greenblatt et al., 2005). This can be seen in Fig. 18, showing the instantaneous velocity field predictions by LES for different phase angles. It displays generation, rolling up and shedding of the vortices through the phase angles of 90° (blowing peak), 180° (switch from blowing to suction), 270° (suction peak) and 360° (switch from suction to blowing). By careful inspection of this figure one can discern the movement of separation point as found in the experiment of Greenblat et al. At the instant corresponding to the blowing peak the local separation zone moves upstream towards the slot, the shear layer being lifted off the wall. As the suction peak is reached, the shear layer is pulled towards the wall and separation point moves downstream of the slot. Concerning existence

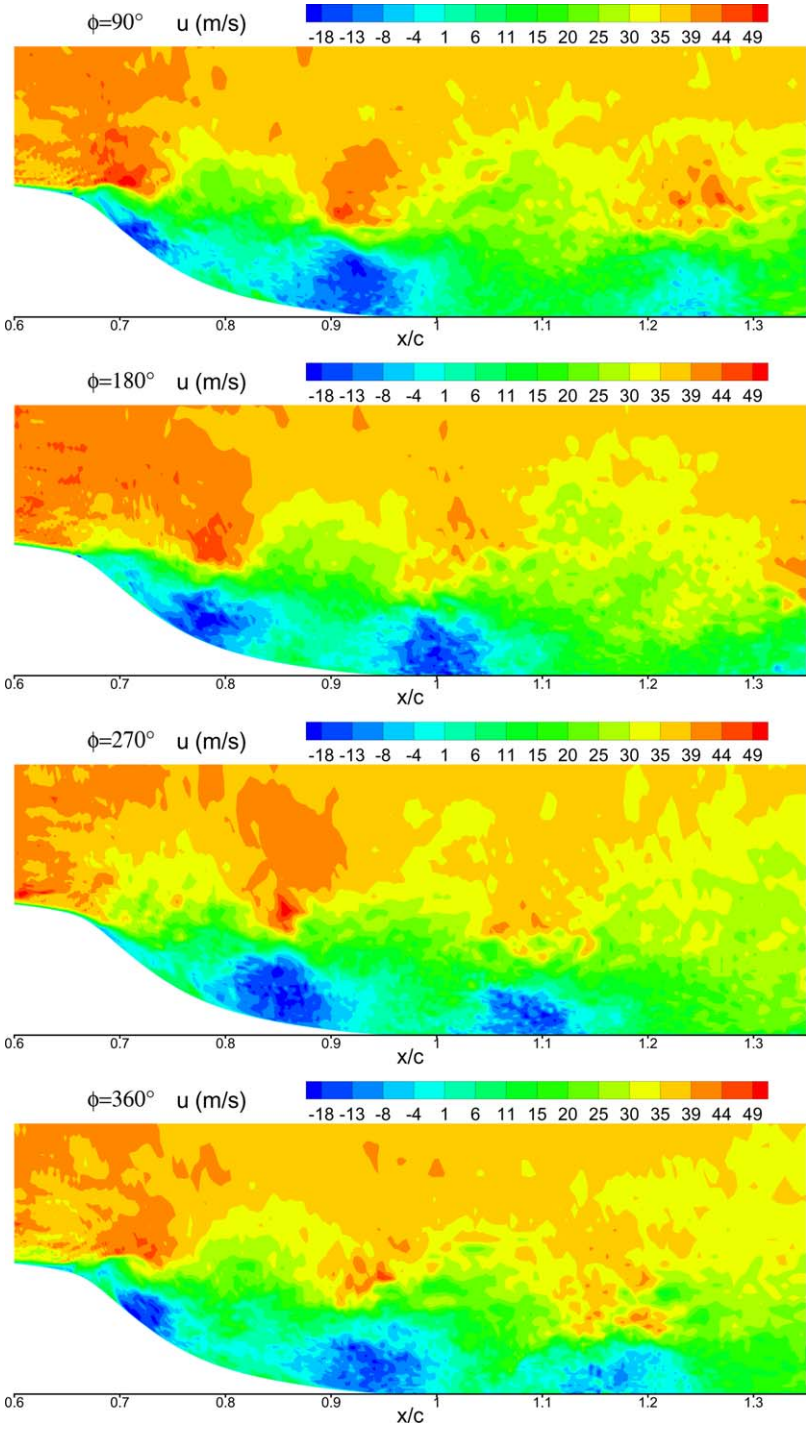

Fig. 18. Instantaneous *U*-velocity field obtained by LES for various phase angles.

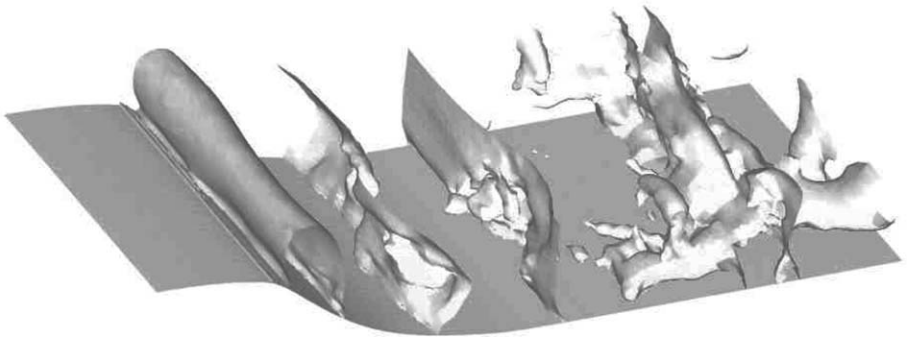

Fig. 19. Iso-surfaces of the pressure fluctuation obtained by DES of oscillatory suction/blowing flow control case.

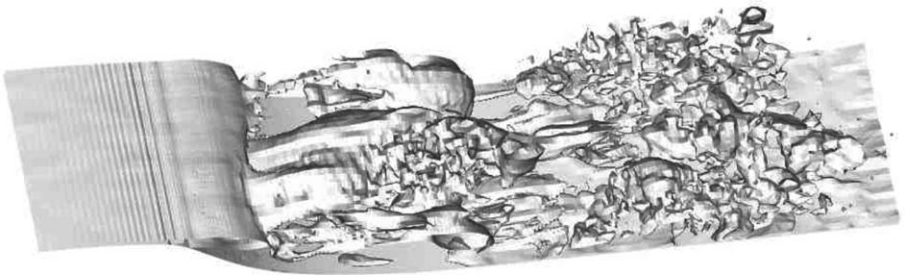

Fig. 20. Iso-surfaces of the spanwise vorticity obtained by DES of oscillatory suction/blowing flow control case.

Fig. 21. Iso-surfaces of the streamwise vorticity obtained by DES of oscillatory suction/blowing flow control case.

of two to three vortices within the instantaneous recirculation zone, a similar observation in the periodically perturbed backward-facing step flow was reported by Yoshioka et al. (2001). Isosurfaces of the instantaneous pressure fluctuation obtained by DES support this observation as shown in Fig. 19. This visualization shows the rolled-up spanwise vortex, which is formed in the region of the control slot, experiencing disruption due to high streamwise vorticity just downstream of the slot. One can observe that the oscillatory control mechanism tends to reorientate the spanwise vorticity field into streamwise vortices. This can be explained by increased velocity fluctuations in the separated shear layer, in both the wall-normal and particularly spanwise direction (not shown here). In order to elucidate coherent flow structures, isosurfaces of vorticity are displayed in Figs. 20 and 21. The DES treatment of the separated region results in clearly visible resolved vortical structures. Evolution of the large-scale spanwise vortices downstream of the slot is observed as a result of the imposed oscillatory perturbation (Fig. 20). Despite an effectively two-dimensional flow field, the three-dimensional instantaneous flow structures (vortices disrupted in the spanwise direction) can be identified. Evidently, the spanwise domain of $0.2c$ employed for DES appears to be sufficient for capturing streamwise vortices displayed in Fig. 21.

4. Conclusions

Different computational approaches: LES (large eddy simulation), DES (detached eddy simulations) and RANS (Reynolds-averaged Navier–Stokes) were used to predict the flow over a wall-mounted hump aiming at comparative analysis of their features and performances in such complex flow situations relevant to the aircraft aerodynamics. In addition to the baseline case, the computations of the

two configurations with active flow control realized by steady suction and oscillatory blowing/suction through a narrow opening (1.7 mm wide) at the hump crest close to the natural separation point were performed. Among the flow configurations considered, the oscillatory case appears to be the most challenging one for the unsteady flow computational strategies like LES and DES.

The LES and DES predictions of the main characteristics of separated flow over a wall-mounted hump, obtained on relatively coarse grids with respect to the flow Reynolds number considered ($Re_c = 9.36 \times 10^5$), are encouraging, outperforming significantly the examined RANS models. As it was expected, the RANS approach was not capable of capturing the dynamics of the large scale motion being especially pronounced in the separated shear layer. A typical outcome is expressed in a lower turbulence level in this flow region leading consequently to a larger recirculation zone and decreased sensitivity against perturbations. LES provided good predictions of the important effects of steady suction and oscillatory suction/blowing flow control, i.e. a shortening of the recirculation bubble compared to the reference baseline case. The DES results are almost identical to those obtained by using the conventional LES in the baseline case. It is especially encouraging when one knows that a substantially lower grid resolution (only 1.7 Mio. cells in total vs. 4 Mio. cells for LES) was applied. However, poor performance in the suction case (LES superior to DES) indicates the importance of the DES grid design with respect to this controlled flow featuring a thinner boundary layer upstream of the separation. The issue of RANS/LES interface appears to be crucial for exploiting advantages of both RANS and LES strategies in different regions of the flow. A comparison of the interface position in all three flow configurations gives a rise to the question whether a grid used for the baseline case can be used for different flow control scenarios, i.e. suction and oscillatory flow control?

Simulations of the oscillatory case demonstrate in general good predictions of the recirculation bubble, both instantaneously and in the time mean sense. Close agreement with the experiment is observed regarding the velocity and shear stress profiles. Despite relatively coarse grid resolution and a narrow computational domain in the spanwise direction ($L_{z,\mathrm{LES}} = 0.152c$ and $L_{z,\mathrm{DES}} = 0.2c$), it was possible to capture the three-dimensional instantaneous flow structures. Finally, appropriate modelling of the slot boundary condition is essential for capturing the mean flow and turbulence characteristics within the recirculation zone.

Acknowledgements

The authors gratefully acknowledge financial support of the Deutsche Forschungsgemeinschaft through the grants GK "Modelling and numerical description of technical flows" and the research group on "LES of complex flows" (FOR 507/1, JA 941/7-1) (S.Š.) and of the German Academic Exchange Service (DAAD) through the "*Sur-Place*" stipend program for Bosnia Hercegovina (A.Dj.).

References

Chun, K.B., Sung, H.J., 1996. Control of turbulent separated flow over a backward-facing step. Experiments in Fluids 21, 417–426.

Dejoan, A., Jang, Y.-J., Leschziner, M., 2005. Comparative LES and unsteady RANS computations for a periodically-perturbed separated flow over a backward-facing step. ASME Journal of Fluids Engineering 127 (3), 872–878.

Fröhlich, J., Mellen, C.P., Rodi, W., Temmerman, L., Leschziner, M.A., 2005. Highly resolved large-eddy simulation of separated flow in a channel with streamwise periodic constrictions. Journal of Fluid Mechanics 526, 19–66.

Gatski, T., Rumsey, C. 2004. CFD validation of synthetic jets and turbulent separation control. Langley Research Center Workshop, Williamsburg, VA, USA, March 29–31.

Gibson, M.M., Launder, B.E., 1978. Grounds effects on pressure fluctuations in the atmospheric boundary layer. Journal of Fluid Mechanics 86, 491–511.

Greenblatt, D., Paschal, K.B., Yao, C.S., Harris, J., Schaeffler, N.W., Washburn, A.E. 2004. A separation control CFD validation test case, Part 1: baseline and steady suction, AIAA Paper No. 2004-2220.

Greenblatt, D., Paschal, K.B., Yao, C.S., and Harris, J., 2005. A separation control CFD validation test case, Part 2: zero efflux oscillatory blowing, AIAA Paper No. 2005-0485.

Hanjalić, K., Jakirlić, S., 1998. Contribution towards the second-moment closure modelling of separating turbulent flows. Computers and Fluids 22 (2), 137–156.

Hanjalić, K., 2005. Will RANS survive LES. A view of perspectives. ASME Journal of Fluids Engineering 127 (3), 831–839.

Jakirlić, S., Hanjalić, K., 2002. A new approach to modelling near-wall turbulence energy and stress dissipation. Journal of Fluid Mechanics 539, 139–166.

Jakirlić, S., Jester-Zürker, R., Tropea, C. 2002. Report on 9th ERCOFTAC/IAHR/COST Workshop on Refined Turbulence Modelling. October, 9–10, 2001, Darmstadt University of Technology, ERCOFTAC Bulletin, No. 55, pp. 36–43.

Jin, S., Choi, H., Kim, S., Yul, Y.-J., Kim, S.-R., 2001. An experimental study of turbulent backward-facing step flow under two-frequency forcing. In: Celata et al. (Eds.), Experimental Heat Transfer, Fluid Mechanics and Thermodynamics. Edizioni ETS, Pisa, pp. 1933–1938.

Johansson, G., Davidson, L. 2005. In: Proceedings of 11th ERCOFTAC/IAHR/COST Workshop on Refined Turbulence Modelling. April 7–8, Chalmers University of Technology, Gothenburg, Sweden.

Klebanoff, P.S. 1954. Characteristics of Turbulence in a Boundary Layer with Zero Pressure Gradient. NACA TN 3178.

Krishnan, V., Squires, K.D., Forsythe, J.R., 2004. Prediction of Separated Flow Characteristics over a Hump using RANS and DES, AIAA Paper No. 2004-2224.

Launder, B.E., Sharma, B.I., 1974. Application of the energy-dissipation model of turbulence to the calculation of flow near a spinning disc. Letters in Heat and Mass Transfer 1, 131–138.

Mason, P.J., Callen, N.S., 1986. On the magnitude of the subgrid-scale eddy coefficient in large-eddy simulations of turbulent channel flow. Journal of Fluid Mechanics 162, 439–462.

Šarić, S., Jakirlić, S., Tropea, C., 2005. A periodically-perturbed backward-facing step flow by means of LES, DES and T-RANS: an example of flow separation control. ASME Journal of Fluids Engineering 127 (3), 879–887.

Seifert, A., Pack, L.G., 1999. Oscillatory control of separation at high Reynolds numbers. AIAA Journal 37 (9), 1062–1071.

Seifert, A., Pack, L.G., 2002. Active flow separation control on wall-mounted hump at high Reynolds numbers. AIAA Journal 40 (7), 1363–1372.

Smagorinsky, J., 1963. General circulation experiments with the primitive equations. Monthly Weather Review 91, 99–164.

Spalart, P.R., 1988. Direct simulation of a turbulent boundary layer up to $R_\theta = 1410$. Journal of Fluid Mechanics 187, 61–98.

Spalart, P.R., Allmaras, S.R., 1994. A one-equation turbulence model for aerodynamic flows. La Recherche Aerospatiale (1).

Travin, A., Shur, M., Strelets, M., Spalart, P.R. 2002. Physical and numerical upgrades in the detached-eddy simulation of complex turbulent flow. In: Friedrich, R., Rodi, W., (Eds.), Fluid Mechanics and its Application, vol. 65, pp. 239–254.

Yoshioka, S., Obi, S., Masuda, S., 2001. Organized vortex motion in periodically perturbed separated flow over a backward-facing step. International Journal of Heat and Fluid Flow 22, 301–307.